RADIAL VARIATION OF THE SOLAR WIND PROTON TEMPERATURE: HEAT FLOW OR ADDITION?

J. D. SCUDDER
Department of Physics and Astronomy, University of Iowa, IA, USA; jack-scudder@uiowa.edu

ABSTRACT

The proton temperature profile of the asymptotic solar wind plasma can be modified by four different physical effects: PdV work, external heat deposition, ΔQ, divergence of heat, $\nabla \cdot \mathbf{q}$, and collisional energy exchange with other species in the plasma. Suggestions in the literature that ΔQ heating is "required" to explain the proton profile have often been deduced while neglecting $\mathbf{q}_p$ and energy exchange. Despite the adiabatic approximation $\mathbf{q}_p = 0$ having no rigorous justification in low-density plasmas, the simultaneous neglect of energy exchange *unnaturally* forces the "need" for ΔQ to balance adiabatic cooling caused by the wind's expansion. In this paper, the asymptotic wind proton heat flux is determined which balances the inner Heliosphere's steady state entropy equation for the protons, ignoring heat addition and energy exchange. The solutions of the energy equation recover both the power-law trend and amplitude of the 5 year averaged *Helios* temperature profiles that were segregated by speed. The dimensionless skewness $\mathcal{S}$ of the heat flow is empirically shown to scale for all wind states below $600 \, \mathrm{km \, s^{-1}}$ as if it were equal to the Knudsen number determined by Coulomb collisions, a relation that is rigorously demonstrated for an infinitesimal Knudsen number, bridging the unusual adiabatic protons for $U \simeq 250 \, \mathrm{km \, s^{-1}}$ and the higher speed states of the winds that remain hotter over a wider radial domain. Higher speed states ($U > 650 \, \mathrm{km \, s^{-1}}$) may require additional scattering beyond what Coulomb effects can provide, although the averaged profiles for these speeds are not as accurate as those below $600 \, \mathrm{km \, s^{-1}}$.

Key words: conduction – equation of state – hydrodynamics – plasmas – solar wind – waves

1. INTRODUCTION

From the earliest measurements, it has been suggested that the proton temperatures in the solar wind were *not* those predicted by a spherically symmetric thermodynamically adiabatic expansion, which has a profile $T_p(r) \propto r^{-4/3}$. In the initial interpretive Phase 1, spherically symmetric two fluid models with Spitzer transport could not predict the ion temperatures observed at Earth for typical wind speeds (Hartle & Barnes 1970). Historically such observations were interpreted as evidence that the protons were being heated by some external agent(s) not in the modeled equations, with wave dissipation suggested. The *Helios* radial profiles opened Phase 2 of the interpretations; they re-enforced the disagreement with the adiabatic predictions (Schwenn et al. 1981; Marsch et al. 1982) and also noted the different radial behaviors of the wind as a function of the size of the solar wind speed, U. The long-lived *Helios* mission produced over 5 years of data involving 34 separate traverses of $0.3 \leqslant r \leqslant 1$ AU. In Phase 2, the inner heliosphere's proton radial variation versus speed state was characterized by Marsch et al. (1983), Schwartz & Marsch (1983), Lopez & Freeman (1986, 1987), Freeman & Lopez (1985), Hellinger et al. (2011, 2013), among others. Lopez & Freeman characterized best-fit radial power laws versus U using all 5 years of *Helios* data as summarized in Figure 1. The most heavily oversampled regime was the 300–600 $\mathrm{km \, s^{-1}}$ states.

The reported inverse radial power-law exponent, $\gamma \equiv -d\ln T_p/d\ln r$, ranged from the "adiabatic" value of $\gamma = 4/3$ (indicated by the red dashed line) at the lowest speeds seen, to generally much shallower radial variations as U increased. The purpose of this paper is to explore the *possible* range of conclusions that come from such inner heliosphere observations.

2. PHASES OF INTERPRETATION OF $T_P(R)$

Theoretically, the variation of $T_j(r)$ in the asymptotic wind regime ($U \simeq U_\infty$) is shaped by 4 factors: (i) work done on its volume element $P_j dV$ ($\pm$); (ii) energy deposition/loss $\Delta Q_j \pm$; (iii) divergence of heat flux $\nabla \cdot \mathbf{q}_j \pm$; (iv) energy exchange ν_{ij} with other plasma components $\pm$, including thermal forces. At the overview level, $T_p(r)$ is less than 1% of the solar wind budget in a Mach 10 flow. Explaining and recovering the radial variation of this small and decreasing fraction requires an accurate and complete physical picture that is likely to involve *all* of the factors listed above.

At times, the proton ($j = p$) budget has been looked at alone, as part of the overall turbulent fluid, or as one of two fluid constituents of solar wind. Confusingly, at different times and in different papers, various subsets of these four factors for protons (and sometimes for the electrons subset) have been explored when interpreting and modeling the solar wind; there has also been some evolution with time in the assessments of the importance of the usually ignored terms. At other times, there has been no clear statement that the paper's conclusions were contingent on the omissions of these other factors, leaving the casual reader with the impression that the paper's stated conclusions have no other reasonable interpretation(s). In setting the context for this paper, a brief overview of the tacit assumptions of various examples of approaches to explaining the proton's observed radial behavior will be presented. This discussion is not meant to review all approaches, but to illustrate the current state of the analysis.

2.1. Phases 1–3

Some Phase 1 interpretations proceeded from the observation that expansion cooling (effect (i)) did not explain the observed $T_p(r)$, and so heat addition (effect (ii)) is required. Other interpretations in this phase included two fluid modeling
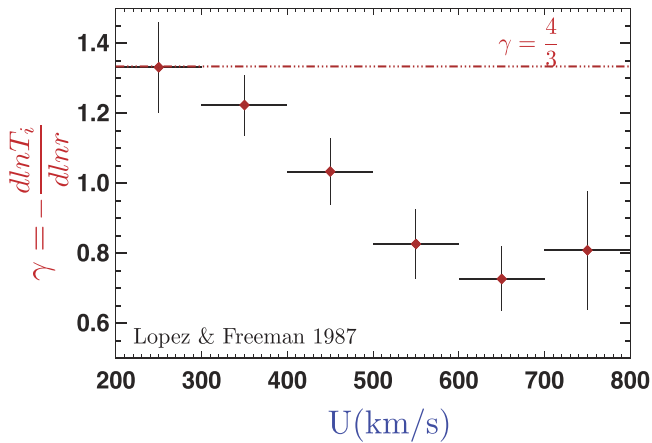
Figure 1. Summary of least squares fits to radial power laws, $T_p \propto r^{-\gamma}$, for *Helios* (1974–1980) as a function solar wind speed state, U (Lopez & Freeman 1986). Error bars and latest updated values are used (Lopez & Freeman 1987). Intervals of ± 50 km about the labeled speed were used for this analysis. Uncertainties indicated reflect the speed intervals and the reported errors for the exponents (Lopez & Freeman 1987).

including effects (i), (iii), and (iv), using Spitzer closure for protons and electrons, but neglecting compressive PdV effects to reach a similar conclusion. In hindsight, such conclusions are parametric (in the first instance) to being able to exclude the occurrence of effects (iii) and (iv), or (in the second instance) to authenticating the correctness of the Spitzer transport used for both electrons and ions, or (in either approach) to excluding the role of positive PdV work in the fluid parcels being modeled.

Phase 2 analysis incorporated the fitted radial power-law variation fits to the *trend* of the proton heat fluxes determined from *Helios* data, $q_p^H(r)$, and six other parameters in the internal energy equation, but ignored the pdV>0 effects of stream dynamics in (i) and did not consider thermal force forms of energy exchange, enroute to concluding that (ii) the data still require external heating. Conclusions of this type are parametric in the assumption that the "...model independent..." characterizations of the *Helios* proton heat flux were sufficiently precise to leverage their conclusions. We return to this assumption below.

Phase 3 of the explanation of $T_p(r)$ has centered on the possible role of turbulent dissipation in the proton heat budget. Three branches of investigation have made contributions: (1) one branch has focussed on modeling the observed features of the proton temperature anisotropy, attributing it to various damping effects ΔQ (e.g., Isenberg & Vasquez 2007; Chandran et al. 2011) of an imposed wave source; (2) another branch has estimated the energy migration via turbulent cascades to shorter scales with a lumped parameter description with a significant list of free parameters that assumes the protons are the ultimate receptacle of the energy cascade generated internally by the solar winds (e.g., Zank et al. 1996; Smith et al. 2001). The dominant sources of turbulence are modeled from estimates of the lumped parameter effects of wind shears and pick-up ions. (3) A third branch has used empirical electron heat flux closures to estimate how the presumed ΔQ energy introduced to the explain the $T_p(r)$ profile would need to be apportioned between electrons and ions (Breech et al. 2009; Cranmer et al. 2009).

All but one of the cited papers in the Phase 3 discussion have ignored (a) the role of the proton heat flux or argued that the proton heat flux was ignorable after first modeling the skew of the VDF as being caused by a delta function moving at the Alfvén speed along $\hat{b}$; the one paper that formally retained the proton heat flux did so with a local closure approximation much in a local form of Grad, while also retaining the Spitzer formulation in the lowest corona for the electron heat flux well outside its domain of validity (see Scudder & Karimabadi 2013). The papers of the Phase 3 discussion also (b) have neglected the role of compressive heating, (i), in the trended data used for closure or constraint, (c) have ignored the thermal force-type exchange terms while sometimes choosing ad hoc energy exchange rates, and (d) have noted, but otherwise ignored, the possibility (Dmitruk et al. 2004; Karimabadi et al. 2014) that the turbulent cascades might be interdicted before depositing their energy in the proton heating and recent evidence (Marino et al. 2008) that the cascades are not omnipresent as initial modeling presumed.

Branch 2 and one of the 3rd branch approaches of Phase 3 rely on a system of lumped parameter equations of turbulence transport that contain a substantial number of free parameters which are adjusted to reach their conclusions. Among these parameters are those which mock up the amount of shear present in the "system," its symmetries, the rate of local production of newborn pick-up ions feeding the turbulence levels, as well as boundary conditions for the domain being modeled. The pick-up effects according to this modeling seem to be most pronounced beyond 20 AU. The other driving mechanism of the turbulence picture is shear, which is most pronounced with the wrapping caused by stream dynamics outside of 1 AU. Among the estimates of the second branch is a semi-empirical digest between 3 and 4 AU that estimates the energy transfer rate of the cascade to the plasma (Marino et al. 2008). In addition to suggesting that the cascade could not completely support the simultaneously measured proton temperature (even if it all went directly there), they also indicated that the energy transfers attributed to the cascades were not always present.

The most detailed and extensive radial analysis has been performed for the *Voyager* intervals, where incidents of pick-up ion effects have been identified beyond 20 AU, where $T_p(r)$ is seen to increase with radius, using careful baselining with 1 AU observations. The pick-up ions drive turbulence in this regime, but turbulence caused by shear would appear to be inadequately supplied in the inner heliosphere to be effective and is thus most effective after the stream–stream dynamics start wrapping up their characteristics, and successive streams and ejecta start overtaking one another beyond 1 AU.

There appears to be a desire in the literature to homogenize all of the radial domains of the solar wind's proton profile as being determined by wave-driven turbulence, despite the almost certain diminution of the effectiveness of pick-up ions and stream driven shears inside of 1 AU. In the inner heliosphere alternate mechanisms have been examined (e.g., Cranmer et al. 2007; Isenberg & Vasquez 2007; Chandran et al. 2011), usually assuming a posited wave spectrum of wave power at the base of the corona. While the proton heat flux (effect (iii)) is formally present in Chandran et al. (2011), it is based on a low-order truncation much in the same spirit as Spitzer's expansion, except here it is about an anisotropic ion distribution. Although the proton heat flux is "...formally.."

present, its physical accuracy is unclear for the same reasons that Spitzer proton transport would be inappropriate. In other references cited (including in the outer heliosphere), this proton heat flux competition has not even been considered as a possible competitor for the turbulence explanation via effect (ii).

Inner Heliosphere Phase 2 work merged theoretical arguments and radial power-law fits to observed plasma moments in order to investigate the balance of the proton energy equation and infer, by subtraction, the missing ingredients that such an analysis suggests must come from ΔQ mechanisms that involve heating or cooling of the protons. These calculations appear at first inspection to involve a complete attempt (except thermal force effects and compressive effects) to look at the balance of the proton internal energy equation. However, as with any experimental arguments, all of these conclusions are parametric in the assumed accuracy of the key observable quantities that provide the leverage for the final scientific evaluation. The proton heat flux $q_p(r)$ plays this role in the conclusions reported by Marsch et al. (1983) and Hellinger et al. (2011, 2013). As argued in this paper, the systematically low value of the *Helios* determination of the proton heat flux, $q_p^H(r)$, leaves even the structurally complete forms of Phase 2 analysis with no clear conclusions.

2.2. Phase 4 $T_p(r)$ Determined by the Proton Heat Flux?

While the Spitzer–Braginskii formulae for heat flow are readily available for electrons and ions, it has taken some time to internalize their not being applicable anywhere in the Heliosphere. Several models retain the Spitzer form for low altitudes in the corona, which arguably even has the wrong sense; in so doing, it builds in a significant conduction loss from the coronal maximum layers back down to the transition region. Even though these predictions of heat flow are now known to be unreliable, there remains the impression that their magnitudes can still be used to estimate their importance. The theoretical assumption underlying Spitzer–Braginskii is that the Knudsen number, K_n, of the species is perturbatively small: $K_n \ll 1$, which is vacated within $\Delta R \simeq 0.05 R_\odot$ above the transition region (Scudder & Karimabadi 2013). Spitzer's estimate for q_e is structurally as well as quantitatively inadequate. Spitzer's estimate of the size of q_p is much more inappropriate and inaccurate, since the the proton $K_{n,p}$ is so much larger than even the electron $K_{n,e}$, and thus further away from the perturbative values required for Spitzer's analysis.

Nonetheless, the small value of Spitzer's formula for the proton heat flow has caused many to ignore the potential role of the ion heat flux in the variation of the ion temperature profile in the solar wind. Others have demonstrated that the proton heat flow in a collisionless supersonic flow might be negligible, starting with Maxwellian boundary conditions (Hollweg 1971; Schulz & Eviatar 1972). Still others have looked at the role of the speed dependence of binary collisions in controlling the skewness (Livi & Marsch 1987), and others have ignored Coulomb effects altogether considering other effects to dominate the mean free path for protons, especially in the far reaches of the Heliosphere (Williams 1995).

This paper experimentally looks at the possibility that the proton heat flux implied by the well-documented *Helios* temperature variation summarized in Figure 1 could determine the size of the proton heat flux, assuming that divergence of the proton heat flux (effect (iii)) is the *only* competition for the

adiabatic cooling of effect (i), while explicitly assuming that there is no ΔQ effect involved and that collisional exchange effects (iv) for the protons are negligible. The likelihood that nature behaves in this way *in the inner Heliosphere* is then tested in the three distinct ways discussed below. While comparing the present solutions $q_p^{TE}(r)$ with the empirical profile reported by *Helios*, $q_p^H(r)$, a *strong systematic shortfall* was identified in the *Helios* determinations of $q_p^H(r)$. This *systematic* finding concerning the *Helios* heat flux implies that those arguments constructed under Phases 2 or 3 that relied on the insufficiency of the *Helios*-determined $\nabla \cdot q_p^H$ (or ignored its contribution) to reach their published conclusions concerning heat addition are no longer valid.

3. MODEL FOR THE SOLAR WIND VARIATION OF $T_p(r, U)$

To illustrate the possible effects of proton heat flux, in this section, we develop a model for the ion heat conduction and illustrate its use in the ion energy equation. The model for the ion heat flux takes the form

$$q_p = \mathcal{S} n M w_p^3 \hat{b}, \tag{1}$$

where $\mathcal{S}$, n, M, and w_p are the skewness, the proton mass, the density, and their rms thermal speed, respectively. This form represents an energy density of the order of the ion pressure making progress in the rest frame with a propagation speed of the ion thermal speed as amplified by the skewness.

Some might refer to Equation (1) as the *saturated heat flux* form, however, the situation is actually the reverse: the saturated form starts from a dimensional argument like Equation (1) and then attempts to suggest the size of $\mathcal{S}$ based on various surmises and, in some cases, calculations concerning instabilities in the presence of certain model forms for the distribution functions. *Any* proton heat flux can be written in this form with $\mathcal{S}$ being a dimensionless number that is to be determined. By adopting this form, there is no presumption of which stochastic effect(s) control the size of q_p. It is clear that $\mathcal{S} \downarrow 0$ is the condition that attends thermodynamic adiabaticity. Geometrically $\mathcal{S}$ reflects the average skewness of the velocity distribution in the proper frame where there is no mass flux. When the heat flow approaches zero, the skewness, or pearshaped nature, of $f(w = v - U)$ goes to zero.

Inserting the general moment form for the heat flux into that of Equation (1), we obtain

$$q_\parallel = \left\langle \frac{1}{2} M \left| v - U_p \right|^2 \hat{b} \cdot \left(v - U_p \right) \right\rangle \equiv \mathcal{S} M n w_p^3, \tag{2}$$

which leaves our dimensionless skew, $\mathcal{S}$, given by

$$\mathcal{S} = \int \left(\frac{w_p^3}{2n} f(v) \right) \left(\frac{\left| v - U_p \right|^2 \hat{b} \cdot \left(v - U_p \right)}{w_p^3} \right) \left(\frac{d^3 v}{w_p^3} \right). \tag{3}$$

Equation (3) shows that the motivation for the form of Equation (1) is to measure parts of the integrand in dimensionless thermal speed units, that is, $\eta = |v - U| / w_p$. *If the speed range of support for $f(w)$ is of order w_p*, as in a Gaussian of half width w_p, the skewness can be expected to be

small, since the integrand is then the product of several factors that are all small relative to unity.

In textbook kinetic regimes, $\mathcal{S}$ is small because it is proportional to the small expansion parameter of these theories, which invariably expand $f(v)$ about local Gaussians. For future consideration, it is well to notice that in such regimes where Spitzer formulations for q_j are valid, it may be rewritten in the form of Equation (1):

$$|\boldsymbol{q}_p| = 3.9 \frac{n\tau k_B T_p}{M} \nabla T_p = O(1) K_n M n w_p^3, \qquad (4)$$

where τ is the collision time, $K_n \equiv \lambda_{mfp}/L$ is the Knudsen number for the collisions that isotropize the distribution, and $\lambda_{mfp} = \tau w_p$. Equations (1) and (4) suggest the close association between skewness and Knudsen number that can explicitly be checked in the Spitzer–Braginskii limit:

$$\mathcal{S} \propto K_n. \qquad (5)$$

This insight is more general than the Spitzer–Braginskii formulae, suggesting that the controlling aspects of skewness are the controllers of the Knudsen number. Even the *"collisionless"* solar wind has some binary collisions that limit its Knudsen number until other, more effective scattering agents are identified. Whatever sets the realized free path for momentum transport will shape the skewness, and hence the heat flux. Because the proton Coulomb Knudsen number can be large, there is every reason to expect that the skewness can be much larger than those regimes of textbooks that insist (for *their* mathematics) on $K_n \ll 1$.

Rather than solve the kinetic equation to predict $\mathcal{S}$, we adopt Equation (1) ensuring that its units are correct and the product of two terms: one that summarizes collisionality via the skewness, and the other that approximates the energy flux density available to carry the heat. In this sense, this modeling does *not* have a specific transport agent in mind, just that it is very hard to stop such an energy flow, other than when the scattering physics effectively makes the mean free path very short compared to the scale lengths of the fluid. It is also possible that a mixture of scattering processes, including waves, set the size of $\mathcal{S}$. However, a baseline maximum of K_n is provided by Coulomb collisions (that never disappear) *with possible effects from waves superposed*, not necessarily as suppliers of heat but as scattering agents moderating the heat flow that would otherwise occur with particles following only Coulomb interdicted collisionless trajectories as discussed by Livi & Marsch (1987). The empirical approach of this paper up to this point, using Equation (1) and the *Helios* profiles, does not commit to a specific process. We show below that when $\mathcal{S}$ is inferred from the 5 year averaged *Helios* data, it is an orderly function of bulk speed (see Figure 4)

After we demonstrate that the proton heat flow might be attractive to explain the reported radial variations in Section 4, we discuss in Section 5 the theoretical and measured indications that q_p is too small to be of consequence.

4. SOLUTIONS

We model the wind in the *Helios* radial range as having a constant speed U_o. By ignoring coupling to electrons and external ion energy sources in the asymptotic uniform flow
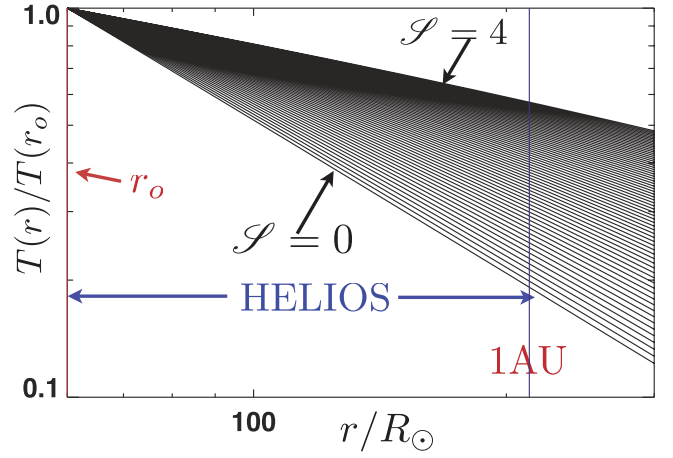
Figure 2. Numerical solutions of solutions to Equation (7) for a range of $\mathcal{S}$ values for a fixed assumed thermal mach number $\mathcal{M} = 10$ at $60R_\odot$. Numerical solutions closely follow the small argument power law behavior of Equation (6). Digests of power law behavior for all $\mathcal{S}$ and $\mathcal{M}$ variations are displayed as separate symbols in Figure 3 below.

regime, the ion internal energy equation takes the form

$$\frac{dT_p}{dr} = -\frac{4}{3} \frac{T_p}{r} - \frac{2}{3nk_B U_o} \nabla \cdot \boldsymbol{q}_p, \qquad (6)$$

where k_B is Boltzmann's constant and U_o is the assumed asymptotic wind speed. After using Equation (1) for $\boldsymbol{q}_p$ and treating $\mathcal{S}$ as constant (that possibly depends on U_o), and the magnetic field in the radial direction, Equation (3) has the solution

$$\ln \frac{T_p(r)}{T_o(\beta)} + 2\beta \left[\exp \left(\frac{1}{2} \ln \frac{T_p(r)}{T_o(\beta)} \right) - 1 \right] = -\frac{4}{3} \ln \frac{r}{r_o}, \qquad (7)$$

where

$$\beta \equiv \frac{\mathcal{S}}{\mathcal{M}}, \qquad (8)$$

and where $\mathcal{M} = \frac{U_o}{w_o}$ is the ion thermal mach number at r_o, where $w_o \equiv w_p(r_o)$. We consider below the range of thermal mach numbers $4 \leqslant \mathcal{M} \leqslant 10$. Since $\mathcal{M}$ and $\mathcal{S}$ are both assumed constant along a U_o stream line, the only factor that controls the solution of Equation (6) is β. From Equation (6), it is clear that $\mathcal{S} \to 0$ yields the collisional fluid's adiabatic $r^{-4/3}$ profile, while the heat flow implied by a finite positive $\mathcal{S}$ produces shallower radial decreases. In the exponential's small argument regime, we obtain the near power-law form that most proton modelers have used to fit the *Helios* observations:

$$T_p(r) \sim T_o(\beta) \left(\frac{r_o}{r} \right)^{\frac{4}{3+3\beta}}. \qquad (9)$$

The radial profiles for the full nonlinear solutions of Equations (6) and (7) are shown in Figure 2 in a log–log format that emphasizes the near power-law behavior of this solution over the relatively narrow radial range surveyed by *Helios*; separate curves have been determined for $\mathcal{S}$ in the range $0 < \mathcal{S} < 4.0$ assuming $\mathcal{M} = 10$. As expected, the profiles with very small $\mathcal{S}$ tend toward adiabatic behavior,

$$q_p = \mathcal{S} n m w_p^3$$
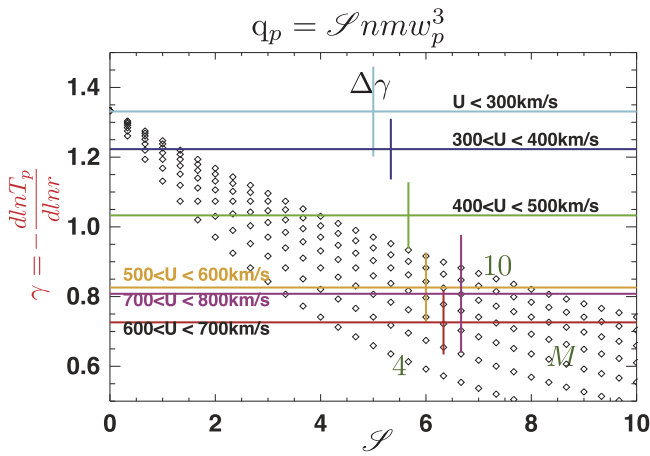
Figure 3. Diamonds represent inverse radial power law exponents for the theoretical solution to Equation (7) with phenomenological heat fluxes, for different combinations of assumptions of $\mathcal{S}$ and $\mathcal{M}$. Diamonds in smooth arcs are results of different $\mathcal{S}$ for fixed, assumed $\mathcal{M}$. A modest range of $\mathcal{S}$ can explain the range of reported proton radial exponents, in the presence of proton heat flow modeled as in Equation (1).

If $\nabla \cdot \mathbf{q}_p$ Determines $T_p(r)$:

Figure 4. Diamonds: inferred dependence $\mathcal{S}(U)$ vs. solar wind speed state required to reproduce the *Helios* 5 years average radial variations (Lopez & Freeman 1986) within their errors (Lopez & Freeman 1987). Diamonds reflect average values of $\mathcal{S}$ considering a range of possible proton mach numbers assumed at $60R_\odot$ ranging from $4 \leqslant \mathcal{M} \leqslant 10$ and the reported statistical uncertainty of the power law exponents. Blue curve shows the independently estimated scaling of $\mathcal{S}(U_o)$ implied by the Coulomb scattering $\lambda_{mfp} \propto T^2/n$ and conserved mass flux dependences: $\lambda_{mfp} \propto U_o^4$.
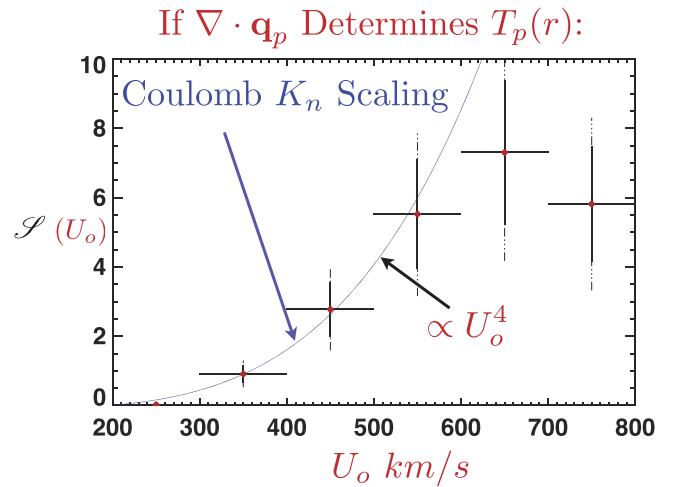
while profiles with larger values of $\mathcal{S}$ have increasingly flatter profiles with radius.

The diamonds in Figure 3 reflect the power-law slope for individual solutions to Equation (7) versus assumed values of $\mathcal{S}$; seven choices of $\mathcal{M}$ [4, 5, …9, 10] at $r_o = 60R_\odot$ generate seven families of curves. The colored horizontal lines reflect the best-fit power laws (by speed range) determined from the fits to 1975–1980 *Helios* data (Lopez & Freeman 1986, 1987). Each horizontal line is labeled with the center solar wind speed used for the fit; fit power-law uncertainties are indicated with flags of the same color as the horizontal line for their best-fit value.

The phenomenological heat flux of Equation (1) can reproduce the experimental *Helios* power laws at different wind speeds provided a necessary dependence of $\mathcal{S}(U_o)$ is chosen; its variation (averaged over the Mach number at fixed speed state) is shown with red diamonds in Figure 4. The horizontal error flags reflect the speed ranges of the fits done by *Helios*. The vertical error flags reflect the impact on the skewness estimates caused by supposing different proton mach numbers at $60R_\odot$, together with the uncertainty of the best-fit *Helios* exponents. As expected, the slow wind is almost adiabatic (with $\mathcal{S}(250) \downarrow 0$), while the higher wind states are suggested to have increasingly skewed distributions. It is important to remember that $\mathcal{S}$ is an empirical parameter determined from assuming Equation (1) and solving the energy equation so that the predicted profile of $T_p^{TE}(r)$ agrees with the logarithmic derivatives of Figure 1 inferred from *Helios* data. Other than assuming $\mathcal{S}$ to be constant along the stream lines of constant bulk speed, no other assumption has been made about the scattering agents that determine its size.

4.1. Does Empirical $\mathcal{S}$ Make Sense?

As a baseline for interpreting Figure 3, we consider the scaling of $\mathcal{S}$ *if* Coulomb processes were controlling the Knudsen number. The temperature and density control λ_{mfp} and the scale length L is proportion to the radius. It is well known that the proton temperature and bulk velocity are strongly correlated as $T_p^{1/2} \propto U$ (Burlaga & Ogilvie 1970), while in the asymptotic wind $nr^2 = C$ so that *for Coulomb*

scattering we can estimate

$$K_{n,p} = \frac{\lambda_{mfp}}{L} \propto \frac{T_p^2}{nr} \propto r U_o^4. \tag{10}$$

Since U_o varies by more than a factor of three across the *Helios* data set, it, rather than r, controls the variation of $K_{n,p}$ across the *Helios* orbit by a ratio of 27:1. If only Coulomb effects were present across all speed states, then these arguments would suggest that a strong U_o^4 dependence should be recovered from the theoretical modeling discussed above.

Motivated by our discussion of $\mathcal{S} \simeq K_n$, in Figure 4 we have over plotted the Coulomb form from Equation (10) via the relation $\mathcal{S} \propto (U/U_*)^4$ over our direct determinations of $\mathcal{S}(U_o)$ (red diamonds), which were obtained from the energy equation and *Helios* data without committing to the actual scattering agent. The lowest four speed states of the six examined fit this relation nearly perfectly (with $U_* \simeq 350\,\mathrm{km\,s}^{-1}$), compatible with the progression toward adiabatic behavior as $U_o \downarrow 250\,\mathrm{km\,s}^{-1}$. In the two highest speed states that have been summarized, a reduction from the Coulomb allowed skewness, or at least a leveling off, is required to explain the radial gradients. This might be a regime where the waves that are present play a role in throttling the otherwise large skew by the scattering they might cause. Note that such scattering need not be interchangeable with suggesting the waves as an energy source. A possible caveat must be considered since Lopez & Freeman explicitly make note of strong oversampling in the data between 300–600 km s^{-1}; one thing that can occur if many of the samples in these radial buckets are from a few of the 34 *Helios* I and II traverses is that the reported radial power law fits (cf. Figure 1) may not be as free of compressional PdV effects or other transient phenoma as in the more oversampled regions (cf Figure 1 in Freeman 1988). These possibilities do *not* detract from the strong and nearly perfect support of the heat flux hypothesis for Coulomb moderated skewness shown by the $U_o < 600\,\mathrm{km\,s}^{-1}$ regime, which is the most oversampled
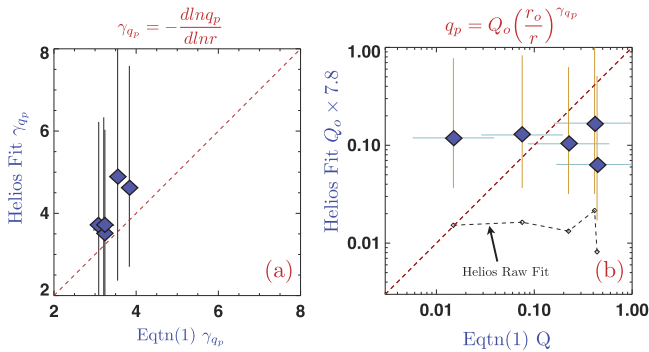
Figure 5. Comparison of radial power law exponents (a) and amplitudes (b) for the *Helios* heat flux profiles and those found to be needed via Equation (1) to explain the long term *Helios* radial power law behaviors of proton temperature.

and, arguably, the *Helios* data most free from compressive and transient phenomena that our spherically symmetric time stationary modeling would not accommodate.

4.2. Do Theory and Observations of $q_p(r)$ Agree?

If the observed temperature profile has $\gamma(U_o) \equiv -\frac{d\ln T_p}{dr}$, then the proton heat flux implied by Equation (1) should have a radial variation

$$q_p(U, r) \propto \mathcal{S}(U) n T_p^{3/2} \propto \mathcal{S}(U) r^{-(3.2:4)}, \quad (11)$$

where the shallowest gradient goes with the higher speed wind and -4 goes with the adiabatic slow wind. Note that the size of the heat flow depends both on the product of the speed dependent skew and the radial variation of the ion thermal speed. In the adiabatic regime, the vanishing of the heat flux comes from the extreme reduction of skewness caused by $K_n \downarrow 0$.

As will become clear below, we are interested in separately comparing the amplitudes $Q(U_o)$ and exponent γ_q when representing $q_p(r)$ as

$$\left| q_p(U_o, r) \right| = Q(U_o) \left(\frac{r_o}{r} \right)^{\gamma_q(U_o)}. \quad (12)$$

We will show that the logarithmic derivatives of q_p, i.e., γ_qs, are nearly the same between *Helios* reported values and the theoretical curves determined from the energy equation fits above. At the same time, we will document that the *Helios* determinations of $Q(U_o)$s are significantly smaller than those from the model explored in this paper.

4.3. Logarithmic Derivatives

We fit the reported *Helios* binned variation of the proton heat flux with results shown in Figure 5(a) and (b). These power-law fits have been performed using the generalized least-squares approach for errors in ordinate and abscissa discussed by Press(1992). The log–log fit addresses the bucket widths in radius for the *Helios* presentation; as no errors are presented for the proton heat fluxes or their standard deviations (as they are bucket averages), we have assumed that the fractional errors for the heat flux are at least as large as those acknowledged for the temperature (Marsch et al. 1983). Actually, the heat flux

determination as a cancellation is probably not as accurate as the even moments associated with the pressure. The temperature fractional error was reported to be 30%, and for these fits we assume 50% uncertainty for the reported proton heat flux.

Below, we discuss the fact that the *Helios* proton heat fluxes are systematically low by factors of 4–12 with typical values of 7.8. This rescaling does not affect the best-fit power-law index. At this adjusted level, the determination is assumed to be 50% accurate. The entire fit space is mapped and the minimum of χ_ν^2 is determined. The 68% errors for the intercept and slope errors were determined by the extremities of the level surface of $\chi_\nu^2 = 2.3$. The steep slope of the fractionally uncertain heat flow's variation with r, coupled with the half decade of variation in $\log r$ and the uncertainty of the abscissa, conspire to give the best-fit power-law exponents a rather wide range of equivalent possibilities.

For the present, we focus on Figure 5(a), which compares the best-fit power-law indices from *Helios* data and those that are required by our model in Equation (1). The fit slopes (i.e., exponents) are consistent with equality, with the best agreement occurring in the higher speed states where the modeled skew was higher.

Figure 5(b) shows two traces for the amplitude Q_o from fitting the *Helios* data versus the amplitudes Q_o which Equation (1) implied from the heat flow that reproduces the observed radial gradient of the proton temperature. The dotted lines connecting the black diamonds are our best-fit amplitudes from fitting the *unmodified Helios* heat flux integrals summarized in the literature (Marsch et al. 1983). These amplitudes are much lower than those expected for Equation (1) to explain the temperature gradients.

As we discuss in Section 5, there is a very strong systematic tendency for the *Helios* heat flux to be smaller than what is actually present in the medium. The shortfall is estimated to be of the order of 780%; that is, the true ambient heat flux is of the order of 7.8 times the inventoried value as a result of this systematic effect. The blue diamonds with orange error flags in the abscissa and ordinate in Figure 5(b) reflect the suggested revised values for the *Helios* information, provided the study presented next is truly representative of all of the situations surveyed by the presented *Helios* data. While the most probable value is 7.8, this factor ranges from 4–12. With these considerations, the Q_o amplitudes from the corrected *Helios* data and the implications of Equation (1) would be consistent.

5. MEASURING THE ION HEAT FLUX

The original *Helios* analysis considered the role of the ion heat flux, $q_p^H(r)$, as determined by numerical integration of the proton-extracted distributions and concluded that it was inadequate to explain the observed profiles of the ion temperature (Marsch et al. 1983). According to their *presented best-fit curves* with unknown treatment of errors or ambiguities in ln r, the heat flux was within a factor of 3–5 of being adequate to explain the temperature variations and an order of magnitude deficient in low-speed winds. As we have just shown in Figure 5, the errors on the best-fit ordinates and abscissae are substantial and high-quality fits require that we inform the optimization process of the errors known to be in the data; these uncertainties were apparently not used in characterizing the *Helios* assessment of the importance of the heat flux. Nonetheless, as we have shown in Figure 5, more appropriate estimates of the heat flow provide amplitudes (black diamonds

connected by dotted line) that are substantially *below* that needed to explain the temperature variation proposed in this paper. However, these fits did show that the radial variation needed for the present approach were consistent with the radial trends of the data Figure 5(a). We now look carefully at the *Helios* approach for determining the proton heat flux from their E/Z measurement by numerical integration.

5.1. E/Z Measurements for Ions: Systematics that Impact Proton Heat Flux

Most 3D proton plasma detectors, like the *Helios* sensors, are variants of detectors that filter charged particles by their energy per unit charge, E/Z, and direction of arrival, rather than filtering the flux based on their mass or the charge state of the particles, such as is done with time of flight mass spectrometry. In the solar wind, the dominant ions are protons and α particles with four times the proton mass and carrying two charges.

When the protons are measured in the solar wind within a narrow range of energy per unit charge $E/Z|_k$ of an electrostatic analyzer, there is an intrinsic degeneracy whereby *different* ions with *different* charges and potentially *different masses* can be collected in the same telemetry window of $\Delta(E/Z)|_k$, provided that the ions arrive from the selected common bundle of directions in velocity space within the field of view set by entrance apertures and deflectors. If the energy per charge is the same for two different charge states, then the accepted velocities of the two species that are found in the same E/Z bucket have the algebraic vector relationship given by

$$U_p + w_p = \sqrt{\frac{M_j Z_p}{M_p Z_j}}\left(U_j + w_j\right), \qquad (13)$$

where U_k and w_k are the bulk velocity and random velocity *vectors* of the k-th species. Since the bulk motions of different species can only drift differentially along $\hat{b}$, this condition may be restated as

$$U_p + w_p = \sqrt{\frac{M_j Z_p}{M_p Z_j}}\left(U_p + \Delta_{j,p} + w_j\right), \qquad (14)$$

where $\Delta_{jp} = U_j - U_p = \zeta_{jp}\hat{b}$ is the field aligned slippage between commonly observed species.

Focusing on contamination from α particles, this condition becomes

$$U_p + w_p = \sqrt{2}\left(U_p + \Delta_{\alpha p} + w_\alpha\right) \qquad (15)$$

or, assuming the proton bulk velocity is in the radial direction,

$$w_p = \left(\sqrt{2} - 1\right)U_p\hat{r} + \sqrt{2}\,\Delta_{\alpha,p} + \sqrt{2}w_\alpha. \qquad (16)$$

If $w_p = \tau w_o\hat{b}$, then the matching conditions become

$$\tau w_o = \left(\sqrt{2} - 1\right)U_p\cos\chi + \sqrt{2}\zeta_{\alpha,p} + \sqrt{2}w_{\alpha,\parallel} \qquad (17)$$

and

$$\left(\sqrt{2} - 1\right)U_p \times \hat{b} = \sqrt{2}w_\alpha \times \hat{b}, \qquad (18)$$

where $\cos\chi = \hat{r}\cdot\hat{b}$ and α particle gyrotropy has been assumed.

Assuming the proton and α thermal speeds are equal to $w_o(r)$ and isotropic, we can write these conditions in terms of

dimensionless thermal speed variables, $\bar{\nu} = \frac{w_j}{w_o}$, of the alphas and protons, that is,

$$\left|\nu_{\alpha,\perp}\right| \simeq 0.2928\mathcal{M}(r)\sin\chi(r) \qquad (19)$$

and

$$\nu_{\alpha,\parallel} \simeq 0.707\tau - 0.2928\mathcal{M}(r)\cos\chi(r) - \sqrt{\frac{\beta_p(r)}{1 + 4\frac{n_\alpha}{n_p}}}, \qquad (20)$$

where gyrotropy has been assumed and the slippage between species is assumed to be at the local Alfvén speed, $V_A^2 = B^2/(4\pi m_p(n_p + 4n_\alpha))$ and $\beta_p \equiv 8\pi n_p k_B T_p/B^2$.

The act of observation of solar wind ions through an E/Z lens induces ambiguity in the information about the plasma obtained with an E/Z sensor. The basic telemetered information of particle counts C_Σ arriving from a given direction θ_v, ϕ_v and collected in a narrow window about $E/Z|_k$ is an *irreducible, entropy producing* sum:

$$C_\Sigma = C_p + \Sigma_j C_j, \qquad (21)$$

where the summation over all counts from species other than protons are from those *different* phase space locales, the mass and charge states, that satisfy Equation (13).

Two different approaches to this problem have been employed: (a) the forward modeling approach, which assumes $f(v_j)$ for all of the modeled species and then predicts the counts that should be collected as a function of the free parameters of such a model; and (b) the other approach seeks to determine the moments of $f(v)$ from a "reasonable approach" that first separates the telemetered counts and assigns them to different species. From the perspective of this paper, both approaches have liabilities; the first produces answers that are optimizations for the fit space assumed, while the second approach determines the answers by numerical integration, provided the count rate matrix is partitioned appropriately. As we have argued above, the process of passing through the E/Z detector is the source of some essential ambiguities in the count rate matrix. Neither method affects a "lossless" reversal of this entropy caused by this form of data collection.

5.2. Proton α Particle Specifics

In this brief section, we focus on the two most common charge states, protons and α particles, He^{++}, which tend to have the *least* overlap in E/Z. Figure 6 illustrates the nature of the measurements for an E/Z detector. The typical situation in the solar wind is that the α particles are observed to slip along the magnetic field and lead the protons as they leave the Sun. In addition, the α particles and protons are commonly observed to have comparable thermal speeds $w_p \simeq w_a$ leading to temperatures proportional to their mass. Typically, the α particles represent 4% by number, with a range of 2%–10%.

As conceptually shown in insets A and B of Figure 6, the protons and α particles occupy their own velocity space. However, the nature of the E/Z sensor is that parts of the α phase space and those of the protons overlap in energy per unit charge, which is the basic "tuning" parameter that the electrostatic analyzer differentiates according to Equations
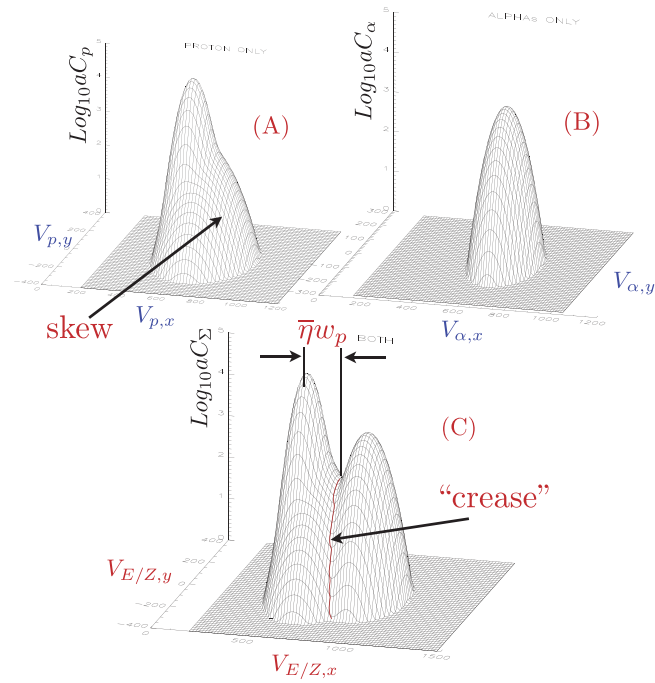
Figure 6. Insets (A) and (B) display count rate matrices for separate proton and alpha particle phase spaces. Bottom inset illustrates how these two conceptually separate phase spaces are "mixed" by an E/Z detector, creating a count rate matrix (C) that is placed in telemetry and must be separated into its separate constituents before clear moments can be determined from either species. Carrying a heat flux, the proton distribution in (A) is skewed. This asymmetry along the magnetic field is preferentially submerged in the saddle point region under the α particle counts where the two separate count rates overlap (inset (C)). This saddle point is about 2.5 proton thermal speeds above the proton bulk velocity peak. The "crease" mentioned in the text is the path of steepest descent down from the saddle point, shown here in red. In the *Helios* data processing, counts below the "crease" are labeled protons and those above the "crease" are alphas, which effectively drops the proton velocity distribution to zero above the crease along $\hat{\boldsymbol{b}}$. Examples of the effect of this procedure are shown in Figure 8 below.

(14) and (16). As shown in inset (C) of this figure, the telemetered count rate matrix is an unknown mix of phase space contributions *in each pixel* of $\langle E/Z \rangle$ and direction of arrival. "Operations" must be undertaken on the composite C_Σ matrix to differentiate the likely contributors that went into each element of the matrix. Thus, as an inverse problem, one has the numerical matrix of inset (C) and would like to extract the respective numerical matrices for the constituent masses and charges corresponding to insets (A) and (B). Like most inverse problems, the answer is not unique but procedures have been described to operationally unpack the third inset into candidate input matrices. As one can see from this figure where the protons are modeled as possessing a heat flux shown by the skewness in their counting rates, this feature of the protons is found "under" the αs and may become lost in the inverse problem under discussion.

The supersonic nature of the wind (relative to ion thermal speeds) implies that the speed v^* of the peak counting rate for each supersonic species is nearly at its bulk speed $(v^* = U(1 + 4\mathcal{M}^{-2}))$, or at its implied energy per unit charge speed in the lower panel. The α peak and proton peak will be separated by $(\sqrt{2} - 1)U_p$, as seen in the lower inset of this figure. However, the ion velocity distribution functions are not

Dirac delta functions, but have probability distributions that cause counts from both species to be found in the "saddle point" region between the two bulk velocity peaks. The number of particles in the vicinity of these thermal spreads determine the anisotropy and heat fluxes of the respective species. As also shown in inset (C), the thermal spreads of the αs and protons overlap, and there are many pixels where the "entropy" caused by the sum created by the detector must be "undone" by data processing on the ground. Some have approached this problem by fitting assumed model forms (such as a superposition of convecting, anisotropic Gaussians) to the underlying distribution functions (Feldman et al. 1973). These techniques must secure their model's parameters for $f_p(v)$ under the α particles as constrained by observations elsewhere, and rely heavily on the appropriateness of the model chosen for that occurring in nature. The *Helios* team avoided fitting functions altogether, wishing to determine the moments of the constituents by numerical integration after first assigning a partition of the count rate matrix. Aside from semantics, it should be clear that such an assignment involves the same kind of judgement, (different) ambiguities, and lack of uniqueness for the information determined in this way as found by those using explicit modeling in the forward modeling approach.

5.3. Estimating Typical Values for "Crease" Speed

Operationally, there is usually a "crease" in the composite count rate spectrum (indicated in red in Figure 6(C)) that passes through the saddle point in the count rates, which gives some idea of the cross over location of dominance between species' count contributions. This crease must be located (in three-dimensions) and a first approach (Marsch et al. 1982) assumes that the makeup of C_Σ is all protons on the low E/Z side of the crease and all α particles on the other side, closer to the second peak. (This general approach was checked by comparing this separation with an electrometer that measured the current, rather than the counts, and showing that this ratio was close to two for that part of the counts identified as *predominantly* α particles. It should be noted that this measurement was designed to differentiate 2 from 1, but not 1.85 from 2, for example. Thus, the extensions of the proton phase space under the alphas, even with these checks, could still have occurred.) It should be carefully noted that this procedure is equivalent to making the $f(v)$ for the two species zero on the corresponding "other" side of this dividing "crease." This will have important implications below. Both fitting and moments have difficulties with the recovery of $f(v)$ in the vicinity of the "crease," especially when determining how the probability for the protons behaves "under" the dominant region of the other species. Conversely, the parallel temperature of the α particles is also potentially affected by the unpacking of the count rate matrix.

Ordinarily in the moment approach, an examination of the partial sums contributing to the integrals can be used to confirm the operational convergence of the moment in question; the effective truncation of the moments above $v_{\text{"crease"}}$ severely interferes with this internal consistency check for convergence, since the truncation de facto makes the integral convergent to its value obtained when the upper limit exceeds $\bar{\eta} w_p$. Fitting procedures to narrow peaks are well disposed toward obtaining the supersonic flow velocity and the density, but even the trace of the pressure or the pressure anisotropy can be influenced by the adopted operational approach to handling the "crease" area.
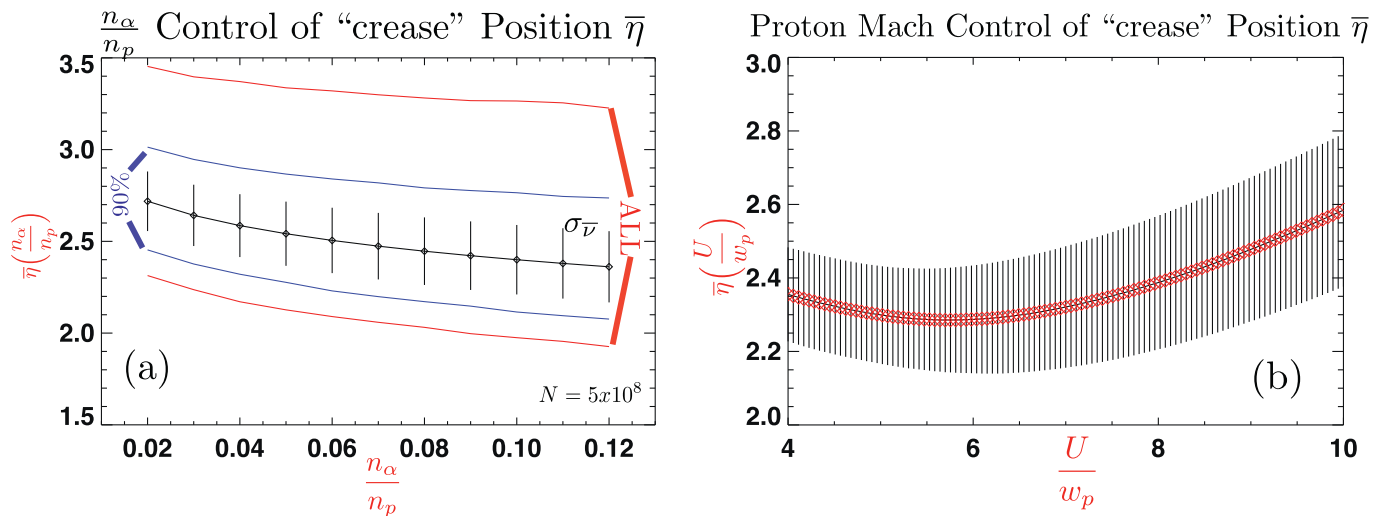
Figure 7. (a) Distribution of $\overline{\eta}$, the average dimensional distance (in thermal speed units) from the peak of the proton velocity to the "crease" along $\hat{b}$ in the E/Z count rate distribution as a function of alpha concentration $\frac{n_\alpha}{n_p}$. Symbols reflect the average and flags the standard deviations at fixed alpha concentrations over a wide range of external parameters that control the overlap and ensuing entropy in the count rate matrix as discussed in the text. This figure summarize one half billion combinations of parameters that cover their expected ranges and combinations over the *Helios* orbit. Blue traces are the boundary including 90% of all outcomes; red curves are the most extreme values (high and low) in the sample. (b) Distribution of $\overline{\eta}$, the average dimensional distance (in thermal speed units along $\hat{b}$) from the peak of the proton velocity to the "crease" in the E/Z count rate distribution as a function of proton thermal mach number. Flags reflect the standard deviation about the means shown.

The heat flux is an extreme example of this type of problem already alluded to by Marsch et al. (1982).

We have used the relations in Equations (17) and (18) to determine the variation of the count rates into an E/Z detector as a function of the increasing proton speed along the magnetic field. At present, we are interested in where the crease intersects the upper limit of $w_\parallel$ for the protons and the overlap of α particles starts to corrupt the clear observations of this part of the protons velocity space. Moving along the ray $\mathbf{v} = \mathbf{U}_o + \eta \langle w^2 \rangle^{1/2} \hat{b}$, we can find where zero pitch angle particles cross the "crease"; its displacement from the proton bulk velocity scaled by the proton rms thermal speed yields the dimensionless offset, η, of the "crease" from the proton bulk velocity, that is,

$$\eta = \frac{\Delta w}{w_o}. \tag{22}$$

This number is of interest since it informs what is the upper, proper frame limit of integration that would have been used in the heat flux integration that we seek to use in Equation (25) below.

As may be seen from Equations (17) and (18), η depends on a rather large number of background parameters: the α-proton concentration ratio, the flow speed, the mach number, the proton beta, and the angle that the magnetic field makes to the radial. We have surveyed nearly half a billion combinations of these parameters for bulk speeds in the range $250 \leqslant U \leqslant 850 \, \text{km s}^{-1}$, proton beta in the range $0.1 < \beta_p < 1$, proton thermal mach number in the range $4 \leqslant \mathcal{M} \leqslant 11$, the angle χ between $\hat{b}$ and the radial in the range $0 \leqslant \chi \leqslant 45°$, and variations of the α concentration from 2% to 10% to determine the likely distribution of the η "crease" locations in proton rms thermal speed units. This range of parameters includes those that would be presented to the *Helios* spacecraft between perihelion and aphelion.

This crease estimate study assumes Gaussians for the ions, and its size could be influenced by yet another quantity—how large is the proton heat flux and in what manner do the protons support this skewness. Since there is at present no clear model for the proton phase space distribution when carrying a given amount of heat, one can generally say that the "crease" speed will increase slightly above our estimate depending on how the heat flow signatures occur in the proton velocity distribution and how much α particle field aligned anisotropy is present in the data.

Figure 7(a) summarizes over a half a billion combinations of parameters that could influence η as a function of the α concentration (which scales the relative heights of the two peaks in Figure 6), and the plotted standard deviations reflect the variability of the crease speed that can be expected. The α concentration produces an orderly, but slight trend for the mean value $\overline{\eta}$ indicated by the black diamonds in this figure. The dispersion about this curve is nearly constant, but the range of η about $\overline{\eta}$ is slightly skewed toward higher values. The red curves indicate the absolute observed extremes in this survey for the crease speed. Nonetheless, this extensive survey shows that typical values for the crease speed are extremely unlikely outside of $2.1 < \eta < 3.22 \pm 0.23$. To routinely obtain convergent heat fluxes by numerical integration, we show in Section 5.4 that uncompromised distribution function coverage until at least $\eta > 5.5$ would appear to be mandatory. When $\eta_{\text{crease}} < 5.5$, the contributions to the integral on $[\nu_{\text{crease}}, 5.5]$ are (i) substantial and (ii) uninventoried in the *Helios* "model independent" determination of the heat flux moment with limits set by the crease determination.

5.4. Impact of $\overline{\nu}$ on Heat Flux Determination by Numerical Integration

We now wish to illustrate the nature of this systematic loss of information and what impact it has on model independent numerical integration for the proton heat flux. A well-known

property of the moments is that their integrands are systematically dominated by contributions that migrate to larger and larger random speeds about the bulk speed as the moment number increases. For our present purposes, we will discuss the density, momentum, pressure, and heat flux as having moment numbers of 0–3. Thus, the heat flux integral ordinarily derives its principal contributions further from the origin of velocity space than the temperature, the momentum, or the density. The precise location of these maxima depends on the details of the distribution function. If Spitzer–Braginskii transport is credible, then the maxima for these moments can be worked out analytically (see Scudder & Karimabadi 2013). The main effect can be seen from the form of the moments: $M_n = \int (f(|\boldsymbol{w}|) + \delta f(\boldsymbol{w})) w^{n+2} P_n(\cos(\theta_w)) dw d\Omega_w$, where $\boldsymbol{w} = \boldsymbol{v} - \boldsymbol{U}$ is the velocity space coordinate in a frame at rest with the species bulk speed, where P_n are the Legendre polynomials of the order of n, and δf are the transport induced corrections to the distribution function in the presence of spatial non-uniformity and microscopic forces. Thus, the integrands leave the origin with $f(\boldsymbol{w})$ multiplied by w^{n+2}, which increasingly detunes the value of the integrand to the features of the probability distribution near the origin (because it is flatter and flatter with increasing n). Eventually, the growth of this polynomial in w will compete with the decrease in $f(|\boldsymbol{w}|) + \delta f(\boldsymbol{w})$ as $|\boldsymbol{w}| \uparrow$. For a given distribution function, the location of the maximum contribution may be computed. For the *same* distribution function, the location of the maxima moves to higher speeds as n increases. For the odd heat flux there are two minimaxes, occurring at different and oppositely signed $w_\parallel$.

To illustrate a consequence of the "crease" partition of C_Σ at $v_\parallel = U_\parallel + \bar{\eta} w_o$, we have modeled (Figure 6(A)) a simple proton distribution in Figure 6 that contains a core–halo model for heat flow (with indicated skewness; Feldman et al. 1973). The purpose is not to endorse such a model, but to have a concrete distribution with a known heat flux; with such a concrete example, the impact of the "crease" upper limit for the heat flux can be quantified. As with all skewed distributions, this model form predicts counts more asymmetrically spread in velocity space than does a Gaussian with no skewness. (The counting rate peaks of Figure 6 do not precisely retain the symmetries of their parent probability distribution functions $f(\boldsymbol{v})$, since the counting rates are integrals over speed with weights of v^4, which bias the high speed side counts from a symmetric Gaussian $f(\boldsymbol{v})$ to be slightly asymmetrical.) For supersonic distributions, this effect, while present, is small (see Figure 6(B)) and should contrast with the markedly skewed "skirt" on the modeled proton distribution in Figure 6. When merged in an E/Z detector (inset (C)), this skew signature is partially obscured "under" the location of the α distribution with non-zero width.

The proton heat flux in magnetic field aligned coordinates, takes the form of

$$q_p = \int_{-\infty}^{\infty} Q(w_\parallel) dw_\parallel, \tag{23}$$

where

$$Q(w_\parallel) \equiv 2\pi \int_0^{\infty} f\left(w_\parallel, w_\perp^2\right) \frac{1}{2} m w_\parallel \left(w_\parallel^2 + w_\perp^2\right) w_\perp dw_\perp. \tag{24}$$

Figure 8. Variation of the fraction $f_p(\eta^* w_p)$ of the actual heat flux obtained by integration between $[-\infty, v_\parallel^*]$ for a core halo skewed proton distribution. For alpha concentrations of 4% the statistical zone of the "crease" at $\bar{\eta} w_o$ found in Figures 7(a), (b) is indicated by the lower probability histogram, $P(\bar{\eta})$. This statistically defined regime of $\bar{\eta}$ determines a probability distribution of the fraction of the true heat flux, $P(f_p(\bar{v}))$, that implies an average short fall of $\langle S \rangle = 780\%$. This suggests that if this modeled velocity distribution were realistic that the *Helios* heat flux reported by numerical integration would be too small by an average factor of $\langle S \rangle = 7.8$. This systematic effect is in the summarized proton heat flux moment of the *Helios* data set.

We then examine the fractional value of the proton heat flux's convergence in the form

$$f_p\left(\eta^* w_o\right) = \frac{\int_{-\infty}^{\eta^* w_o} Q(w_\parallel) dw_\parallel}{q_p}. \tag{25}$$

We note that the negative parallel half of the random proton velocity space is unencumbered by other counts from different composition, so that starting the integral for f_p at large negative values of $w_\parallel$ should initially obtain the correct partial integrated values, $Q(w_\parallel < 0)$.

The crucial question then becomes what value does $f_p(\bar{\eta} w_o)$ take on compared to unity? If this number is small, then the *Helios* heat flux would seriously have underestimated the true heat flux by a factor of the order of $f_p^{-1}(\bar{\eta} w_o)$.

The results of this exercise are indicated in Figure 8. For values of $\eta < 0$, the partial integral is negative since the integrand of $Q(w_\parallel)$ contains the odd polynomial $a w_\parallel + |b| |w_\parallel|^3$. As the upper limit of integration goes through $\eta = 0$, the value of the integrand becomes increasingly positive, adding to the total, and the fraction f_p starts reducing its negative size by getting successive positive increments. As the sign changing curve for $f_p(\eta^* w_o)$ indicates, the integral has converged to a positive outward heat flux provided $\eta > 6$. However, the statistical location for $\bar{\eta}$ is rather compact, as shown by its probability distribution $P(\bar{\eta})$ rising off the bottom horizontal axis. By interpolating these results against the master curve for $f_p(\eta^* w_p)$, we can determine the probability distribution $P(f_p(\bar{\eta}))$ in the histogram anchored in the right vertical axis. The fractional convergence factor for the heat flux integral, f_p, is the independent variable of this second probability function. Its shape indicates that the most probable value of $f_p \sim 0.1$ and has a half width of approximately 0.04. While this probability is skewed toward higher values of the fraction (the most

extreme fraction (with probability $1/10^7$) is as high as 0.6), the dominant occupancy of this histogram is certainly below 0.2. This indicates that this effect might suggest shortfalls instead, ranging between $[1/.2, 1/.06] = [5, 16.6]$, with the most likely shortfall being of the order of 10 fold. The actual weighted average of $\langle f_p^{-1} \rangle = 7.8$ was used in constructing the blue diamonds in Figure 5(B), which nicely overlap (with their errors) with the amplitudes suggested from Equation (1) which reproduced the proton temperature radial power laws of the *Helios* data.

Since the α particles always lead the protons along $\hat{\boldsymbol{b}}$ and because the mapping of E/Z tends to place the α peak at speeds $\sqrt{2}\, U_p$, the nature of the α particle entropy systematically occurs on the high proton thermal speed side of the proton bulk speed peak of the distribution. Accordingly, the E/Z systematics (with truncations at $v_{\mathrm{crease}} = \bar{\eta} w_p$) will systematically tend to underestimate the proton heat flux.

There are many variables involved in determining the size of this underestimate; among the prominent factors will be the actual size of the proton and α particle thermal speeds, the actual α concentration, the actual slippage of the alphas along the magnetic field, and the concentration of the alphas relative to the protons. All of these factors impact the precise determination of the "crease." In constructing $P(\eta_{\mathrm{crease}})$ we have surveyed all of these effects except $w_p \neq w_\alpha$. The precise location also depends on *how* the proton distribution is skewed in velocity space.

It appears that short of a 3D mass-differentiated distribution function, the true size of the proton heat flux may not be yet known in a model independent way, certainly not as function of radius from the *Helios* data set.

6. DISCUSSION AND SUMMARY

The present paper has explored the possibility that the proton heat flux and its implicit redistribution of internal energy can explain the observed radial variations of the proton temperature as a function of solar wind speed state. Using Equation (1), we have determined the average skewness required to replicate the long-term *Helios* proton radial variations reported previously; this has been done without any predetermination of the stochastic agents involved in regulating the transport. Independently, we have also estimated the variation of $\mathcal{S}$ that would be expected if it were principally determined only by the Coulomb mean free path λ_{mfp} for scattering; its scaling with bulk speed in the asymptotic wind is (i) strong and (ii) strikingly similar (see Figure 4) to the empirical skewness determined by comparing the radial temperature profiles produced by Equation (1) in the energy equation, being especially precise below $U_o < 600$ km s^{-1}. The deduced variation of skewness, determined by the observed gradients of $T_p(r)$, recovers the expected strong bulk speed dependence that would attend the skewness being set by the Coulomb collisional mean free path that is over plotted in Figure 4. Empirically there seems to be some upper limit set for the skewness of the protons in the highest speed winds that reverse this trend of growth of skewness with proton binary mean free path. This might be a regime where wave particle scattering begins to limit the mean free path of the protons involved. Alternatively, this highest speed regime of the *Helios* catalog is the least well sampled multiple times (see Figure 1, Freeman 1988) and may have more transient compression physics in its average profile. More needs to be done in this area as well. We have recovered the adiabatic behavior of the lowest speeds in the wind within this frame work by inferring a small skewness in such a low-speed state that is consistent with our overall scaling. By way of contrast, to date, the alternate view of external heating for the wind protons has not reproduced the *Helios* radial variations of the protons as a function of speed state.

The proton internal energy budget for the wind is rather small, being $\mathcal{M}^{-2}$ of the ram energy; accordingly, a theory that explains its variation must be fairly accurate and consider carefully all possible contributions. Thermodynamic adiabaticity does not just happen, it requires collisions to ensure that heat conduction does not disrupt this postulated thermal isolation. As shown in Figure 4, the collisionality that enforces very small skewness in the ultra-slow wind produces very weak $\boldsymbol{q}$ and induces adiabatic behavior in the presence of the flux tube's expansion. As shown by the same graph, this argument cannot be sustained in the higher speed winds with the lower densities and higher temperatures which both cause a rapidly growing mean free path for Coulomb collisions that allows heat to flow generally. Proton heat will flow because there are insufficient collisions to impede it from flowing; postulating adiabaticity requires a rationale that is generally not present in the solar wind's expansion.

When considering the "collisionless" solar wind, $U \geqslant 350$ km s^{-1}, the proton heat flow will generally be present and disruptive of thermodynamic adiabatic conditions. Arguments for the necessity of ΔQ in such flows that have postulated adiabatic expansions are inconsistent. When modeling the effectiveness of coronal heating, suitable heat flow models must be included. As shown with the present calculation, $\nabla \cdot \boldsymbol{q}$ is a significant entropy source and is capable of removing the need for ΔQ addition. Early arguments that the observed T_p disagreed with the adiabatic solar wind solution do not actually imply that heating of the ΔQ type is required; instead, they imply that one of the four types of entropy addition discussed in this paper is involved in changing the temperature profile. Unless and until an argument is made that collisional physics supports an insulating adiabatic description, the role of a *relevant* heat flux must be inventoried which is valid for the Knudsen number of the medium being discussed. A relevant model must also predict the *direction* of the heat flux. The accuracy of modeling heat flowing back toward the transition region from coronal maximum clearly impacts the amount of heat required to maintain the corona; however, retaining Spitzer's invalid heat description with its $\boldsymbol{q} = -\kappa \nabla T$ prediction in the low corona while studying the effectiveness of wave damping is just such a disconnect. There are several papers discussed above that do just that!

The radial variations for q_p required by Equation (1) are not inconsistent with the power laws for q_p discussed by *Helios* researchers Marsch et al. (1982). We have refit their presented data assuming that the heat flows have 50% errors, treated the bucketed errors in $\ln r$ properly, and determined heat flux radial exponents with errors that are compared with those required from Equation (1) in our model in Figure 5.

As shown in Figure 8, the parallel velocity space integral for $q_{\parallel,p}$ contains a strong negative contribution from below the solar wind velocity before acquiring its final positive value, if all of velocity space is "in view." That figure shows with $P(\bar{\eta})$ that this moment was routinely interdicted well before it converged. This interdiction at $+2w_p$ occurs for nearly all of the conditions surveyed for the *Helios* mission. Accordingly, the

reported heat flux values from the *Helios* numerical integrations have three properties: (i) though numerically incorrect, they are aligned with $\hat{\boldsymbol{b}}$; (ii) though numerically incorrect, they are proportional to the correct value (by the fixed dimensionless cutoff), so that their radial variation $d\ln q_p^H\big/d\ln r$ should nearly be correct, since this quantity is independent of the proportionality constant; and (iii) the size of q_p^H does leave $\nabla \cdot \boldsymbol{q}_p^{Helios}$ too small in the ion entropy equation for its true contribution.

Given that the α position in *E/Z* rather regularly clips the q_p integral at a comparable number of thermal speeds above the proton peak, the radial variation of q_p^H might be better than its overall estimate of the size of the heat flux. We have shown (Figure 5(a)) that the radial exponents of *Helios* and this paper are compatible, and that, after correcting for an estimate of the shortfall indicated by the α particle "entropy," that the magnitude of the heat flux required by Equation (1) appears to be consistent with the observations (Figure 5(b)). These findings have implications for the significant body of research that has relied on the *Helios* heat flow determinations and their radial variation to sustain their conclusions (Marsch et al. 1983 and Hellinger et al. 2011, 2013).

Other mass-resolved proton spectrometers have been flown in the solar wind on *ACE*, *Ulysses*, and *Stereo*, but determinations of the proton heat flux measurements have not yet been discussed in the literature. With Solar Probe Plus there will be a 3D mass-resolved spectrum (J. Halekas 2015, private communication) for protons, at least at times, that can evaluate the idea that the proton heat flux exceeds what can be determined by generalized "crease" partitions of *E/Z* phase space, which will also be available.

The unusual circumstance of asymptotic wind conditions and many *Helios* passes through a fixed radial regime has allowed the calculation of the proton heat flow necessary to explain the observed temperature profiles—while simultaneously ignoring compressive heating, wave damping, or exchange terms. Arguments have been advanced in connection with Figure 4 of this paper that Coulomb mean free path effects are present in the inner Heliosphere data as the nearly exclusive limiters of the proton heat flux that flows for $U \leqslant 600$ km s^{-1}. For even less collisional, higher-speed winds, other agents (perhaps wave scattering) could play a role in keeping the mean free path from going as high as the proton mean free path would suggest, although the quality of the radial profiles is not as good for these speed ranges as those between 300 and 650 km s^{-1}. These data reenforce the important idea that by weakening collisions one does *not* cause the heat flow to go to zero; rather, the reverse

occurs: the heat flow becomes more important with enhanced skewness (Figure 4) as the system becomes more "collisionless." These data also seem to support the *pro tempore* approach for estimating heat flows in large Knudsen number regimes by using a *form* like Equation (1) that is self similar to, but retains the same structural scaling $\mathcal{S} \simeq K_n$ that can be verified in detail with Spitzer–Braginskii transport in the form of Equation (10) when $K_{n,p}$ is suitably small.

REFERENCES

Breech, B., Matthaeus, W. H., Cranmer, S. R., et al. 2009, JGR, 114, A09103
Burlaga, L. F., & Ogilvie, K. W. 1970, ApJ, 159, 659
Chandran, B. D. G., Dennis, T. J., Quaetert, E., et al. 2011, ApJ, 743, 197
Cranmer, S. R., Asgari-Targhi, M., Miralles, M. P., et al. 2015, RSPTA, in press, arXiv:1412.2307
Cranmer, S. R., Mattheus, W. H., Breech, B. A., et al. 2009, ApJ, 702, 1604
Cranmer, S. R., van Ballegooijen, A. A., & Edgar, R. J. 2007, ApJS, 171, 520
Dmitruk, P., Mattheus, W. H., & Seenu, N. 2004, ApJ, 679, 617
Feldman, W. C., Asbridge, J. R., Bame, S. J., et al. 1973, JGR, 78, 2017
Freeman, J. W. 1988, GeoRL, 15, 88
Freeman, J. W., & Lopez, R. E. 1985, JGR, 90, 9885
Hartle, R. E., & Barnes, A. 1970, JGR, 75, 6915
Hellinger, P., Matteini, L., Stverak, S., et al. 2011, JGR, 116, A09105
Hellinger, P., Travnicek, P., Stverak, S., et al. 2013, JGR, 118, 1351
Hollweg, J. V. 1971, JGR, 76, 7491
Isenberg, P., & Vasquez, B. 2007, ApJ, 668, 546
Karimabadi, H., Roytershteyn, V., Vu, H. X., et al. 2014, PhPl, 21, 3
Livi, S., & Marsch, E. 1987, JGR, 91, 8045
Lopez, R. E., & Freeman, J. W. 1986, JGR, 91, 1701
Lopez, R. E., & Freeman, J. W. 1987, JGR, 92, 13679
Marino, R., Sorriso-Valvo, L., Carbone, V., et al. 2008, ApJL, 677, L71
Marsch, E., Muehlhaeuser, K. H., Rosenbauer, H., et al. 1982, JGR, 87, 52
Marsch, E., Muehlhaeuser, K. H., Rosenbauer, H., et al. 1983, JGR, 88, 2982
Neugebauer, M., & Feldman, W. C. 1979, SoPh, 63, 201
Press, W. H., Teukolsky, S. A., Vetterling, W. T., et al. 1992, in Numerical Recipes in Fortran 77: The Art of Scientific Computing (2nd ed.; Cambridge: Cambridge Univ. Press)
Schulz, M., & Eviatar, A. 1972, CosEl, 2, 402
Schwartz, S. J., & Marsch, E. 1983, JGR, 88, 9919
Schwenn, R., Marsch, E., & Rosenbauer, H. 1981, Solar Wind 4, ed. H. Rosenbauer (Garching: Max-Planck-Institute für Aeronomie), 126
Scudder, J. D., & Karimabadi, H. 2013, ApJ, 770, 26
Smith, C. W., Mattheus, W. H., Zank, G. P., et al. 2001, JGR, 106, 8253
Williams, L. 1995, ApJ, 453, 953
Zank, G. P., Mattheus, W. H., & Smith, C. W. 1996, JGR, 101, 17093